Vibro-Acoustic Simulations of Ships by Coupled Fast BE-FE Approaches

Lothar Gaul[1], Michael Junge[1], Marc Wilken[2], Christian Cabos[2], and Dominik Brunner[1]
[1] Institute for Nonlinear Mechanics, University of Stuttgart, Germany
[2] Germanischer Lloyd, Hamburg, Germany

ABSTRACT

The vibration behavior of ships is noticeably influenced by the surrounding water, which represents a fluid of high density. In this case, the feedback of the fluid pressure onto the structure cannot be neglected and a strong coupling scheme between the fluid domain and the structural domain is necessary. In this work, fast boundary element methods are used to model the semi-infinite fluid domain with the free water surface. Two approaches are compared: A symmetric mixed formulation is applied where a part of the water surface is discretized. The second approach is a formulation with a special half-space fundamental solution, which allows the exact representation of the Dirichlet boundary condition on the free water surface without its discretization. Furthermore, the influence of the compressibility of the water is investigated by comparing the solutions of the Helmholtz and the Laplace equation. The ship itself is modeled with the finite element method. A binary interface to the commercial finite element package ANSYS is used to import the mass matrix and the stiffness matrix. The coupled problems are formulated using Schur complements. To solve the resulting system of equations, a combination of a direct solver for the finite element matrix and a preconditioned GMRES for the overall Schur complement is chosen. The applicability of the approach is demonstrated using a realistic model problem.

Nomenclature

Ω_s, Ω_a	structural domain, acoustic domain
Γ_s, Γ_I	structural boundary, coupling interface
Γ_H	half-space boundary
t_s, t_f	tractions on Γ_s and Γ_I
ϱ_s, λ, μ	structural density, Lamé constants
n	unit normal direction of the fluid domain
u	structural displacements
c_f, ϱ_f	speed of sound and density of the fluid
p, q	acoustic pressure and flux
$\bar{p}$, $\bar{q}$	prescribed pressure and flux
$\tilde{p}$, $\tilde{q}$	unknown pressure and flux
f	excitation frequency
ω, κ	wave number, circular wave number
$P(x,y)$	fundamental solution
$P^*(x,y)$	half-space fundamental solution
V, D	single layer potential, hypersingular operator
K, K'	double layer potential and its adjoint
$\boldsymbol{K}^\mathrm{m}_\mathrm{BE}$, $\boldsymbol{C}^\mathrm{m}_\mathrm{BE}$	Galerkin matrices of mixed formulation
$\boldsymbol{K}^\mathrm{h}_\mathrm{BE}$, $\boldsymbol{C}^\mathrm{h}_\mathrm{BE}$	Galerkin matrices of half-space formulation
$\boldsymbol{K}_\mathrm{FE}$	dynamic stiffness matrix
$\boldsymbol{C}_\mathrm{FE}$	coupling matrix
$\boldsymbol{T}_\mathrm{q}$	transformation matrix
$\boldsymbol{S}$	Schur complement
c_d	near-field parameter
c_e	expansion length parameter
L	expansion length
$h_l^{(1)}$	Hankel functions
P_l	Legendre polynomials
s	far-field direction
D	distance vector between clusters

1 Introduction

Fluid–structure interaction deals with the mutual influence of an acoustic and a structural domain. If air is assumed as acoustic fluid, the influence of the surrounding fluid on the vibration behavior of the structure can usually be neglected. In contrast, this is typically not the case if the fluid is water. Due to its high density, the feedback of the acoustic pressure onto the structure has to be taken into account [5]. As a consequence fully coupled simulation schemes have to be applied which are computationally more expensive, since a structural problem and an acoustic problem have to be solved simultaneously.

For geometrically simple structures, analytical solutions exist [11]. Typically, the structure of engineering problems are more

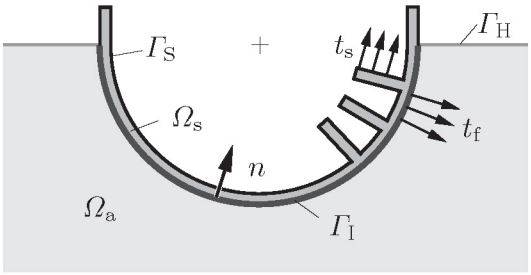

Figure 1: The coupled problem consists of a structural domain Ω_{s} and an acoustic domain Ω_{a}. The two domains are in contact to each other on the fluid-structure interface Γ_{I}. The water surface Γ_{H} is modeled with zero pressure boundary conditions.

complex so that numerical schemes have to be used. The finite element method (FEM) is usually applied for the structural part [17]. For exterior acoustic fluid domains, the application of the boundary element method (BEM) is advantageous, since the Sommerfeld radiation condition is automatically fulfilled [16]. There are fast methods to overcome the drawback of the fully populated matrices like the fast multipole method (FMM) [13, 9] and $\mathcal{H}$-matrices [12]. With these fast methods it is possible to solve large scale problems in acoustics with some thousand degrees of freedom [6, 8]. If ship-like structures are considered, the water surface has to be incorporated. One possibility is to apply a mixed formulation [15] where only a finite part of the water surface in the vicinity of the ship is discretized. Alternatively, a half-space fundamental solution can be applied, which exactly fulfills the boundary condition on the water surface [14]. In this case, only the ship-hull needs to be discretized. There are various formulations for the coupling of the FEM and BEM [6, 10, 1]. Recently, fast BEM approaches were coupled with the FEM [6, 2], allowing the simulation of large–scale coupled problems.

This paper starts with the governing equations of the coupled problem and presents two different formulations for the BEM. After this, the fast multipole method is introduced to accelerate the computations. A FEM representation for the structural part is discussed and a strong coupling scheme is presented. The different approaches are used to examine a realistic model problem. At the end the influence of the compressibility is investigated by comparing the results of the Helmholtz equation with the ones of the Laplace equation.

2 GOVERNING EQUATIONS OF THE COUPLED PROBLEM

In the following, the governing equations for the fluid-structure interaction problem are presented for the time harmonic case with the behavior $\mathrm{e}^{-\mathrm{i}\omega t}$. The wavenumber is denoted by $\omega = 2\,\pi\,f$, where f is the excitation frequency. The structural domain Ω_{s} (cf. Fig. 1) is assumed be linear elastic with the Lamé constants λ and μ. The material is homogeneous with the structural density ϱ_{s}. The corresponding elastodynamic problem for the displacements u is given by

$$\omega^2 \varrho_{\mathrm{s}}\, u(x) + \mu \Delta u(x) + (\lambda + \mu)\,\mathrm{grad}\,\mathrm{div}\, u(x) = 0 \qquad \text{for } x \in \Omega_{\mathrm{s}} \subset \mathbb{R}^3\,, \tag{1}$$

$$T\,u(x) = t_{\mathrm{s}} \qquad \text{for } x \in \Gamma_{\mathrm{s}}\,, \tag{2}$$

and by an additional transmission condition which is introduced later by (6). The Laplacian is denoted by Δ and T represents the traction operator. The structure is excited by the prescribed tractions t_{s}. The acoustic pressure p in the fluid domain Ω_{a} is either described by the time harmonic Helmholtz equation in case of a compressible fluid or by the Laplace equation in case of an incompressible fluid. Since the latter case is obtained by setting the speed of sound $c_{\mathrm{f}} \to \infty$, the derivations are only done for the more general case of the Helmholtz equation. In this paper, a partly immersed structure is investigated where the free fluid surface Γ_{H} is modeled by a Dirichlet boundary condition. The acoustic boundary value problem has the form

$$\Delta p(x) + \kappa^2\, p(x) = 0 \qquad \text{for } x \in \Omega_{\mathrm{a}}, \tag{3}$$

$$p(x) = 0 \qquad \text{for } x \in \Gamma_{\mathrm{H}}\,, \tag{4}$$

$$\left| \frac{\partial p}{\partial R} - \mathrm{i}\,\kappa\, p \right| < \frac{c_{\mathrm{f}}}{R^2} \qquad \text{for } R = |x| \to \infty\,, \tag{5}$$

and an additional transmission condition which is presented later by (7). The circular wavenumber is denoted by $\kappa = \omega/c$. Equation (5) is called Sommerfeld radiation condition, which ensures an outgoing wave within the exterior acoustic domain [7]. Since a fluid with a high density is used, the feedback of the pressure onto the structure is not negligible.

Therefore, a strong coupling scheme has to be applied, which is represented by the two transmission conditions

$$T\,u(x) \;=\; t_{\mathrm{f}}(x) = -p(x)\,n_x \qquad \text{for } x \in \Gamma_{\mathrm{I}}, \tag{6}$$

$$q(x) \;:=\; \frac{\partial p(x)}{\partial n_x} = \omega^2 \varrho_{\mathrm{f}} u(x)\,n_x \quad \text{for } x \in \Gamma_{\mathrm{I}}\,, \tag{7}$$

where the acoustic flux q is introduced. In the next two sections, the mixed BEM formulation and the half-space BEM approach are outlined.

3 MIXED BEM FORMULATION FOR THE ACOUSTIC DOMAIN

One possibility to model the acoustic problem of partly immersed structures is to discretize the water surface in the vicinity close to the structure. On the boundary Γ_{H}, the Dirichlet data vanish, i.e. $p = 0$ holds. Starting point are the boundary integral and the hypersingular boundary integral equation [12]

$$\frac{1}{2}p(x) \;=\; \underbrace{\int_\Gamma P(x,y)\,q(y)\,\mathrm{d}s_y}_{(Vq)(x)} - \underbrace{\int_\Gamma \frac{\partial P(x,y)}{\partial n_y}\,p(y)\,\mathrm{d}s_y}_{(Kp)(x)}\,, \quad x \in \Gamma \tag{8}$$

$$\frac{1}{2}q(x) \;=\; \underbrace{\int_\Gamma \frac{\partial P(x,y)}{\partial n_x}\,q(y)\,\mathrm{d}s_y}_{(K'q)(x)} - \underbrace{\int_\Gamma \frac{\partial^2 P(x,y)}{\partial n_x\,\partial n_y}\,p(y)\,\mathrm{d}s_y}_{-(Dp)(x)}\,, \quad x \in \Gamma \tag{9}$$

which are valid for a general smooth boundary Γ. The single layer potential is denoted by V, K and K' are the double layer potential and its adjoint and D is the hypersingular operator. The free-space fundamental solution is denoted by

$$P(x,y) = \frac{\mathrm{e}^{\mathrm{i}\kappa|x-y|}}{4\pi|x-y|}\,. \tag{10}$$

The pressure and flux are decomposed in a prescribed part $(\bar{\cdot})$ and an unknown part $(\tilde{\cdot})$

$$p(x) = \tilde{p}(x) + \bar{p}(x) \qquad , \qquad q(x) = \tilde{q}(x) + \bar{q}(x)$$
$$\text{with } \begin{cases} \tilde{p}(x) = \bar{q}(x) = 0 & x \in \Gamma_{\mathrm{H}}\,, \\ \bar{p}(x) = \tilde{q}(x) = 0 & x \in \Gamma_{\mathrm{I}}\,. \end{cases} \tag{11}$$

Plugging (11) into (8) and weighting with constant functions ν^q on Γ_{H} yields

$$\begin{aligned} -\int_{\Gamma_{\mathrm{H}}} \nu^q(x)\,(V_{\mathrm{H}}\tilde{q})\,(x)\,\mathrm{d}s_x \;+\; \int_{\Gamma_{\mathrm{H}}} \nu^q(x)\,(K_{\mathrm{I}}\tilde{p})\,(x)\,\mathrm{d}s_x \;= \\ \int_{\Gamma_{\mathrm{H}}} \nu^q(x)\,(V_{\mathrm{I}}\bar{q})\,(x)\,\mathrm{d}s_x \;-\; \int_{\Gamma_{\mathrm{H}}} \frac{1}{2}\nu^q(x)\,\bar{p}(x)\mathrm{d}s_x - \int_{\Gamma_{\mathrm{H}}} \nu^q(x)\,(K_{\mathrm{H}}\bar{p})\,(x)\,\mathrm{d}s_x\,, \end{aligned} \tag{12}$$

where the subscript of the inner operator – H or I – represents the corresponding domain Γ_{H} and Γ_{I}. The same procedure is done on Γ_{I} for the hypersingular boundary integral equation (9) using linear functions ν^p for weighting

$$\begin{aligned} -\int_{\Gamma_{\mathrm{I}}} \nu^p(x)\,(K'_{\mathrm{H}}\tilde{q})\,(x)\,\mathrm{d}s_x \;-\; \int_{\Gamma_{\mathrm{I}}} \nu^p(x)\,(D_{\mathrm{I}}\tilde{p})\,(x)\,\mathrm{d}s_x \;= \\ \int_{\Gamma_{\mathrm{I}}} \nu^p(x)\,(K'_{\mathrm{I}}\bar{q})\,(x)\,\mathrm{d}s_x \;-\; \int_{\Gamma_{\mathrm{I}}} \frac{1}{2}\nu^p(x)\,\bar{q}(x)\mathrm{d}s_x + \int_{\Gamma_{\mathrm{I}}} \nu^p(x)\,(D_{\mathrm{H}}\bar{p})\,(x)\,\mathrm{d}s_x\,. \end{aligned} \tag{13}$$

Introducing a triangulation with piecewise linear shape functions for p and constant ones for q yields the system of equations

$$\underbrace{\begin{pmatrix} \boldsymbol{V}_{\mathrm{HH}} & -\boldsymbol{K}_{\mathrm{HI}} \\ \boldsymbol{K}'_{\mathrm{IH}} & \boldsymbol{D}_{\mathrm{II}} \end{pmatrix}}_{\boldsymbol{K}^{\mathrm{m}}_{\mathrm{BE}}} \begin{pmatrix} \tilde{\boldsymbol{q}} \\ \tilde{\boldsymbol{p}} \end{pmatrix} = \underbrace{\begin{pmatrix} -\boldsymbol{V}_{\mathrm{HI}} \\ \frac{1}{2}\boldsymbol{M}_{\mathrm{I}} - \boldsymbol{K}'_{\mathrm{II}} \end{pmatrix}}_{-\boldsymbol{C}^{\mathrm{m}}_{\mathrm{BE}}} \bar{\boldsymbol{q}}\,, \tag{14}$$

where the boundary condition $\bar{p} = 0$ has already been taken into account. Since not the whole infinity water surface can be discretized, it is desirable to have an formulation where the boundary condition on the water surface is included automatically. This can be achieved using a half-space fundamental solution as outlined in the next section.

4 HALF-SPACE BEM FORMULATION FOR THE ACOUSTIC DOMAIN

As pointed out in [3], the fluid domain which is bounded by the flat water surface can be seen as semi-infinite half-space. For such a problem, the use of the special half-space fundamental solution

$$P^*(x,y) = \frac{1}{4\,\pi}\frac{\mathrm{e}^{\mathrm{i}\,\kappa\,|x-y|}}{|x-y|} - \frac{1}{4\,\pi}\frac{\mathrm{e}^{\mathrm{i}\,\kappa\,|\tilde{x}-y|}}{|\tilde{x}-y|} \tag{15}$$

is advantageous, where x is mirrored on the half-space plane to obtain $\tilde{x}$. If $P^*(x,y)$ is plugged into (8) and (9) it can be shown, that the integrals over the water surface vanish exactly. Thus, the boundary integral equations (8) and (9) are applicable in the same way but this time $P^*(x,y)$ is used instead of $P(x,y)$ and only Γ_I has to be considered [3]. To obtain a Galerkin formulation, both boundary integral equations are weighted with linear functions ν. Again a triangulation with piecewise linear shape functions for p and constant ones for q are applied, leading to

$$\left(\frac{1}{2}\boldsymbol{M} + \boldsymbol{K}\right)\boldsymbol{p} = \boldsymbol{V}\,\bar{\boldsymbol{q}} \qquad \text{and} \qquad -\boldsymbol{D}\,\boldsymbol{p} = \left(-\frac{1}{2}\boldsymbol{M}' + \boldsymbol{K}'\right)\bar{\boldsymbol{q}}\,, \tag{16}$$

where the matrices correspond to the operators introduced in (8) and (9), but this time with the fundamental solution $P^*(x,y)$. For exterior acoustic problems, spurious modes may occur. There are several possibilities to overcome this phenomenon. A widely applied strategy is to use a linear combination of the boundary integral equations (16) with a coupling constant α

$$\underbrace{\left(\frac{1}{2}\boldsymbol{M} + \boldsymbol{K} - \alpha\boldsymbol{D}\right)}_{\boldsymbol{K}^h_{\mathrm{BE}}}\boldsymbol{p} = \underbrace{\left(\boldsymbol{V} - \frac{1}{2}\alpha\boldsymbol{M}' + \alpha\boldsymbol{K}'\right)}_{-\boldsymbol{C}^h_{\mathrm{BE}}}\bar{\boldsymbol{q}}\,, \tag{17}$$

which is known as the Burton-Miller approach. A parameter $\alpha = {}^{-i}/_{\kappa}$ turns out to be stable and advantageous concerning the condition number. On possibility to implement the half-space fundamental solution is to mirror the elements and nodes at the water plane and call the standard integration routines for a combination of y with the non-mirrored point x and a second time for y with the mirrored point $\tilde{x}$. The result of the second integration simply has to be subtracted from the first one and inserted into the global matrices. Besides the additional memory consumption for storing the mirrored elements and nodes, no further increase of the storage requirements occur, since the size of $\boldsymbol{K}^h_{\mathrm{BE}}$ and $\boldsymbol{C}^h_{\mathrm{BE}}$ is not altered. However, for classical BE methods, these matrices are still fully populated. In order to overcome this drawback, the fast multipole method (FMM) is applied. The mirror-technique turns out to be advantageous for the FMM implementation, since the standard expansion can be applied.

5 FAST MULTIPOLE IMPLEMENTATION

For the introduced operators, one typically has to evaluate potentials of the type

$$\Phi(x_b) = \sum_{a=1}^{A}\frac{\mathrm{e}^{\,\mathrm{i}\kappa|x_b-y_a|}}{|x_b-y_a|}q_a, \tag{18}$$

where q_a denotes the source strengths of A sources. Standard BE methods typically consider the interaction of every combination of a load point with a field point. In contrast to this, the multipole algorithm sets up a clustering and sums up the contribution of all sources q_a in the center z_a of a cluster (see Fig. 2 left). At the next step, this so–called far–field signature is translated to the center z_b of the other clusters and from there finally distributed to x_b.

From a mathematical point of view, the separation of the distance $|x_b - y_a|$ in the fundamental solution succeeds by using the diagonal form of the multipole expansion [13]

$$\frac{\mathrm{e}^{\,\mathrm{i}\kappa|x_b-y_a|}}{|x_b-y_a|} = \frac{\mathrm{i}\kappa}{4\,\pi}\sum_{l=0}^{\infty}(2l+1)\,\mathrm{i}^l h_l^{(1)}\left(\kappa|D|\right)\int_{\mathbb{S}^2}\mathrm{e}^{\,\mathrm{i}\kappa(d_a+d_b)\cdot s}P_l\left(s\cdot\hat{D}\right)\mathrm{d}s\,, \tag{19}$$

with the Hankel functions h_l and the Legendre polynomials P_l. The vectors which are local to the clusters are denoted by d_a and d_b (see Fig. 2), whereas D is defined by the centers of two interacting clusters. The unit distance vector is defined by $\hat{D} = {}^{D}/_{|D|}$. The integral over the unit sphere $\mathbb{S}^2$ is approximated by Gauss point quadrature using discrete values of

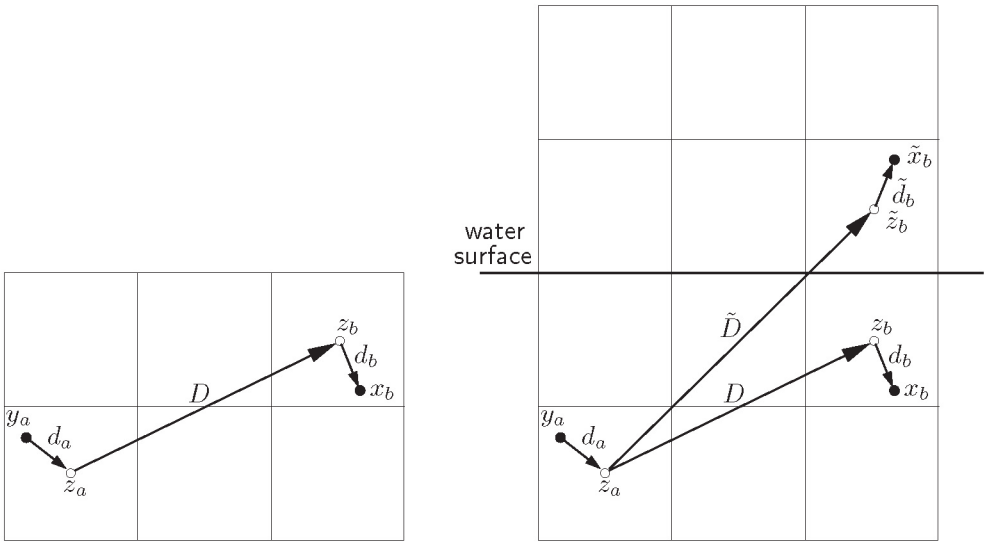

Figure 2: Clustering and splitting up of the vector between load point and field point into three parts for the symmetric formulation left (left) and the half-space formulation with geometrical mirroring (right).

the the far–field directions s [13]. Since one can not compute an infinite sum, the series has to be truncated. In this case the integration over the unit sphere $\mathbb{S}^2$ and the summation can be interchanged. Introducing the translation operator

$$M_L(s, D) = \sum_{\ell=0}^{L} (2\ell + 1)\mathrm{i}^\ell h_\ell^{(1)}(\kappa|D|) P_\ell(s \cdot \hat{D}) \,, \tag{20}$$

the original potential (18) can now be expressed in the form

$$\Phi(x_b) \approx \frac{\mathrm{i}\kappa}{4\pi} \int_{\mathbb{S}^2} \mathrm{e}^{\mathrm{i}\kappa\, d_b \cdot s} M_L(s, D) \underbrace{\sum_{a=1}^{A} \mathrm{e}^{\mathrm{i}\kappa\, d_a \cdot s} q_a}_{F(s)} \,\mathrm{d}s. \tag{21}$$

The choice of L in (20), which is called the *expansion length*, has a significant influence on the accuracy and the performance of the multipole algorithm. Proper choice helps to circumvent divergence of the series and will be discussed later in this section. The sum on the right hand of (21) is called the *far–field signature* $F(s)$. It is local to the cluster with the sources q_a, since only the vector d_a appears. In contrast to this, the translation operator M_L only depends on the vector D between two clusters' centers. Thus, if a regular cluster grid is used, the translation operators can be reused. Translating the far–field signature to another cluster using a translation operator forms the so called *near-field signature*. The solution is finally recovered by an exponential function of d_b and an integration over the unit sphere.

Since the multipole expansion is only valid for well separated load and field points, one has to split up the clusters into a near–field and far–field. All clusters which fulfill the condition

$$|D| < c_d \frac{d}{2} \tag{22}$$

form the near–field. Here, d denotes the cluster diameter and c_d is a constant. The arising near–field is represented by a sparse matrix. It has to be evaluated by classical BEM. All other clusters are in the far–field and form the so called *interaction list*.

To obtain an optimal efficiency, a hierarchical multilevel cluster tree is used. It is set up by consecutive bisectioning such that a mother cluster is divided into two son clusters on the next level. The procedure starts with the *root cluster*, which is the smallest parallelepiped containing all elements of the model. The division is stopped if a specified number of elements per cluster is reached. These final clusters, which do not have any sons, are called *leaf clusters*. The interaction list of every cluster is formed by those clusters, which are in the near-field of the *mother cluster* but not in its own near–field.

Obviously, the far–field signature has to be translated to the interaction lists on different levels. Since the cluster diameters are different on every level, the expansion length L has to be adapted to every level, too. Typically the well–established semi–empirical rule

$$L\left(\kappa\, d_\ell\right) = \kappa d_\ell + c_\mathrm{e} \log\left(\kappa\, d_\ell + \pi\right) \tag{23}$$

is used to estimate the number of series terms on level ℓ of the cluster tree [4]. The parameter c_e has to be chosen by the user and determines the desired accuracy. In order to maintain the accuracy of the multipole expansion when the cluster diameter increases on the next level, an interpolation and filtering strategy has to be applied. It is advantageous to use a fast Fourier transform for this purpose. This is because new far–field directions have to be added, which is only possible for the original form of the multipole expansion [9, 6]. The resulting *fast multipole method* (FMM) has a quasi linear complexity of order $\mathcal{O}(N \log^2 N)$ as outlined in [6].

The evaluation of the matrix-vector product for the symmetric formulation with the FMM algorithm is similar for all operators which are neededed for the coupling formulations. Only slight modifications are necessary in order to take into account the different test and shape functions. The general procedure can be summarized with the following steps:

1. Compute the near-field part by a sparse matrix–vector multiplication.
2. Evaluate the far-field signature $F(s)$ for every leaf cluster.
3. Translate the far-field signature to all interaction cluster by means of the translation operators (Eq. 20) and sum it up as the near–field signature $N(s)$ there.
4. Shift the far-field signature to the mother cluster and repeat step 3 until the interaction list is empty.
5. Go the opposite direction and shift the near-field signature $N(s)$ to the son clusters until the leaf clusters are reached.
6. Recover the solution by integration over the unit sphere.

In case of the half-space problem, modifications are necessary for the near-field and the far-field [3]. The near-field also has to include the interaction to mirrored-clusters, which fulfill the near-field condition with a non-mirrored cluster. The multipole cycle is similar to the one of the symmetric formulation, however in step 3, the far-field signatures $F(s)$ also have to be translated to the mirrored clusters as depicted in Fig. 2 (right). In step 5, the shifting procedure also has to be done for the mirrored clusters. In step 6, the solution additionally needs to be recovered for the mirrored clusters and subtracted from the solution of the corresponding non-mirrored clusters. For a discussion of the computation time, the interesting reader is referred to [3].

6 COUPLED APPROACH

The structural problem given by (1) and (2) is discretized using the finite element method resulting in a system of linear equations

$$\underbrace{\left(-\omega^2 \boldsymbol{M}_\mathrm{s} - \mathrm{i}\omega \boldsymbol{D}_\mathrm{s} + \boldsymbol{K}_\mathrm{s}\right)}_{\boldsymbol{K}_\mathrm{FE}} \boldsymbol{u} = \boldsymbol{f}_\mathrm{s} + \boldsymbol{f}_\mathrm{f}\,, \tag{24}$$

where $\boldsymbol{M}_\mathrm{s}$ and $\boldsymbol{K}_\mathrm{s}$ denote the mass matrix and the stiffness matrix, respectively. In this paper, stiffness proportional damping is considered with the damping matrix

$$\boldsymbol{D}_\mathrm{s} = k_d\, \boldsymbol{K}_\mathrm{s}\,, \tag{25}$$

where k_d denotes a damping parameter. Vector $\boldsymbol{f}_\mathrm{s}$ incorporates the tractions t_s due to the driving forces. The finite element package ANSYS is utilized to set up the matrices $\boldsymbol{M}_\mathrm{s}$, $\boldsymbol{K}_\mathrm{s}$ and the right hand side vector $\boldsymbol{f}_\mathrm{s}$. They are imported into the research code by a binary interface. The data exchange only needs to be done once for a given model, since $\boldsymbol{M}_\mathrm{s}$ and $\boldsymbol{K}_\mathrm{s}$ are frequency independent. Typically, shell elements with six degrees of freedom are applied for thin structures.

The vector $\boldsymbol{f}_\mathrm{f}$ is defined by the first transmission condition (6). The nodal forces are computed from the fluid pressure by

$$\boldsymbol{f}_\mathrm{f} = -\boldsymbol{C}_\mathrm{FE}\,\boldsymbol{p} \qquad \text{where } \boldsymbol{C}_\mathrm{FE} \text{ is assembled from} \qquad \boldsymbol{C}_\mathrm{FE}^k = -\int_{\tau_k} \boldsymbol{N}_u^\mathrm{T}\, \boldsymbol{n}^k\, \boldsymbol{N}_p \,\mathrm{d}s_x\,. \tag{26}$$

The matrix with the structural shape functions is denoted by $\boldsymbol{N}_u$ and the one with the fluid shape functions by $\boldsymbol{N}_p$. According to the second transmission condition (7), the acoustic flux q on each boundary element τ_m is computed from the structural displacements of the adjacent nodes k by

$$\bar{\boldsymbol{q}} = \boldsymbol{T}_q \boldsymbol{u} \qquad \text{where each row is given by} \qquad q_m = \frac{1}{3}\varrho_\mathrm{f}\omega^2 \sum_{k\in m} \boldsymbol{u}_k \cdot \boldsymbol{n}^m\,, \tag{27}$$

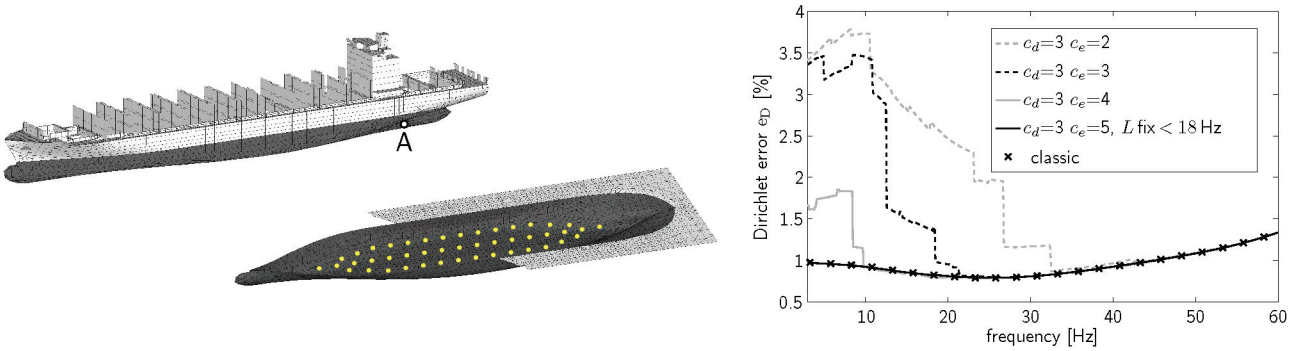

Figure 3: Discretized model of the investigated container-vessel (left top). The wet boundary elements are highlighted in dark gray. For the mixed formulation a part of the water surface is discretized as shown for the rear half. Light spots indicate the position of the used monopole sources (left bottom). Dirichlet error $\mathrm{e_D}$ for the half-space formulation and different multipole parameters (right).

and ϱ_f denotes the density of the fluid. To obtain the coupled system of equations, (26) is plugged into (24) and (27) into (14) or (17) yielding

$$\begin{pmatrix} \boldsymbol{K}_\mathrm{FE} & \boldsymbol{C}_\mathrm{FE} \\ \boldsymbol{C}_\mathrm{BE}\boldsymbol{T}_q & \boldsymbol{K}_\mathrm{BE} \end{pmatrix} \begin{pmatrix} \boldsymbol{u} \\ \boldsymbol{x} \end{pmatrix} = \begin{pmatrix} \boldsymbol{f}_\mathrm{s} \\ 0 \end{pmatrix}, \tag{28}$$

In case of the mixed formulation, $\boldsymbol{K}_\mathrm{BE}^\mathrm{m}$ and $\boldsymbol{C}_\mathrm{BE}^\mathrm{m}$ are used and $\boldsymbol{x} = (\tilde{\boldsymbol{q}}, \tilde{\boldsymbol{p}})^\mathrm{T}$, where $\tilde{\boldsymbol{p}}$ is the unknown pressure on the ship-hull and $\tilde{\boldsymbol{q}}$ is the unknown flux of the elements on Γ_H. For the half-space formulation, $\boldsymbol{K}_\mathrm{BE}^\mathrm{h}$ and $\boldsymbol{C}_\mathrm{BE}^\mathrm{h}$ are used and $\boldsymbol{x} = \boldsymbol{p}$ denotes the pressure on the ship hull. The coupled system (28) is rearranged using the Schur complement $\boldsymbol{S}$

$$\underbrace{\left(\boldsymbol{K}_\mathrm{BE} - \boldsymbol{C}_\mathrm{BE}\boldsymbol{T}_q\,\boldsymbol{K}_\mathrm{FE}^{-1}\boldsymbol{C}_\mathrm{FE}\right)}_{\boldsymbol{S}}\boldsymbol{x} = -\boldsymbol{C}_\mathrm{BE}\boldsymbol{T}_q\,\boldsymbol{K}_\mathrm{FE}^{-1}\boldsymbol{f} \tag{29}$$

and a GMRES is applied to solve for $\boldsymbol{x}$. In each iteration step, $\boldsymbol{K}_\mathrm{FE}^{-1}$ must be applied to a vector. This is efficiently done using a LDL^T factorization, which only has to be computed once and can be reused in each iteration step. For the mixed formulation, a scaling of the different blocks of $\boldsymbol{K}_\mathrm{BE}$ is performed. As preconditioner, an ILU factorization of the near-field matrix of $\boldsymbol{K}_\mathrm{BE}$ is applied.

7 NUMERICAL RESULTS

In this section, the proposed fast BE-FE coupling schemes are compared for the container vessel depicted in Fig. 3 (left top). The model consists of 16547 nodes and 35836 structural degrees of freedom. The number of boundary elements on the ship hull is 2858 and 1343 nodes are in contact with the water. Water with the density $\varrho_\mathrm{f} = 1000\mathrm{kg/m^3}$ and the speed of sound $c_\mathrm{f} = 1483.2\mathrm{m/s}$ is assumed as acoustic fluid. The structure is excited by 691 forces caused by the pressure fluctuations of the ship propeller. For the mixed approach, a rectangular area of the water surface is meshed as shown for the rear half (cf. Fig. 3 left bottom). The minimal distance d_w between the ship hull and the edge of the discretized water surface is chosen from the set {2.5 m, 5 m, 10 m, 20 m, 40 m and 80 m}. For the smallest water area with $d_\mathrm{w} = 2.5\,\mathrm{m}$, 639 nodes are located on the water surface which increases to 11799 nodes in case of the largest model. Before the simulations of the coupled approaches are presented, the BE part of the mixed formulation is compared with the half-space formulation concerning the accuracy and efficiency.

7.1 ACCURACY OF THE FLUID PART

To examine the accuracy of the fluid part, an analytical field is created using 90 monopole sources. Half of them are located within the ship hull as decpicted in Fig. 3 (left bottom). To fulfill the Dirichlet boundary condition on the water surface, the monopole sources are mirrored and the strength multiplied by minus one. For this field, both the pressure and flux are known for a given point and normal direction. Hence, the analytical flux is used as boundary condition $\bar{\boldsymbol{q}}$ and the corresponding pressures $\boldsymbol{p}$ or $\tilde{\boldsymbol{p}}$ at the nodes on Γ_I are computed using (17) or (14). Since the analytical pressure $\boldsymbol{p}_\mathrm{mono}$

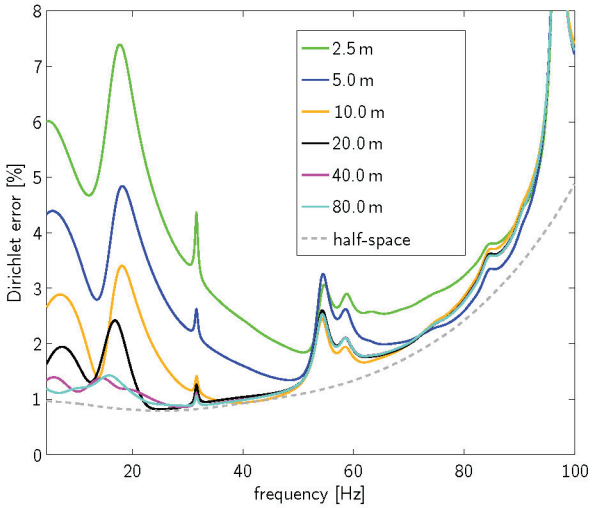

Figure 4: Container-Vessel: The Dirichlet error is visualized for different frequencies. The discretized water area of the mixed formulation is varied between 2.5 m and 80 m. The half-space result is plotted as comparison.

is known, the Dirichlet error

$$\mathrm{e_D} = \frac{||\boldsymbol{p} - \boldsymbol{p}_{\mathrm{mono}}||_{L_2}}{||\boldsymbol{p}_{\mathrm{mono}}||_{L_2}} \tag{30}$$

can be defined. In case of the mixed approach $\tilde{\boldsymbol{p}}$ is used instead of $\boldsymbol{p}$. First, the influence of the multipole parameters c_d and c_e as defined by (22) and (23) is investigated for the half-space formulation. As reference solution, the classical implementation without FMM is utilized. The corresponding Dirichlet errors are depicted in Fig. 3. For small frequencies and small expansion lengths, one observes a larger Dirichlet error. The error can be reduced by increasing the expansion length. A parameter $c_e = 5$ turned out to give a small error, if the expansion length is computed by (23) using a fixed frequency of 18 Hz for all frequencies $f \leq 18$ Hz. For this choice, hardly any difference between the error of the classical implementation and the fast multipole implementation is observable any more. For this reason, this parameter set is chosen for all following simulations.

The Dirichlet errors are also computed for the mixed approach. The discretized water area is varied as mentioned above. The half-space solution is exact in the sense, that the Dirichlet boundary condition on the water surface is incorporated in an exact way and can therefore be seen as the achievable solution. Figure 4 shows the Dirichlet errors within a frequency range from 3 Hz to 100 Hz. All errors of the mixed formulation are larger than the half-space solution. For $d_{\mathrm{w}} = 2.5$ m, the errors reach almost 8% in the region around 20 Hz. The error curves of the mixed approach are wavy in contrast to the half-space formulation. This may lead to misinterpretation especially at 95 Hz where one observes an artificial resonance. If the discretized water area is enlarged, the errors tend to decrease. But this is not generally the case. For instance at a frequency $f = 55$ Hz, the error is almost independent of the discretized water area and approximately twice as large as for the half-space formulation. The same holds for the resonance effect at 95 Hz, which occurs even for the largest water area. Hence, one concludes, that the half-space formulation is superior to the mixed formulation concerning the accuracy.

When using simulation tools for real life applications, also the efficiency is of major interest. Therefore, the computational times and the memory consumptions are discussed in the following. For all simulations a Intel Xeon 5160 CPU with 16GB RAM is used. The computational times for the models with the different water areas are depicted in Fig. 5 (left). The half-space approach does not need to discretize the water surface. Hence, the corresponding computational times are indicated by dashed horizontal lines in the same color. For small water areas with $d_{\mathrm{w}} \leq 10$ m, the mixed formulation is slightly faster concerning the set-up time of the near-field. However, the solution time for the half-space formulation is always smaller compared to the mixed approach. For this reason, the total simulation time including the reading of the model file and writing of the results files is always smaller for the half-space formulation. Thus one concludes, that the half-space formulation is also superior to the mixed formulation in terms of the computational time.

Besides the computational time also the memory consumption is compared. The results are visualized in Fig. 5 (right). Obviously, the near-field of the mixed formulation always requires more memory than the one of the half-space approach. Due to the mirrored mesh, the memory consumption for storing the model information is slightly larger for the half-space formulation compared to the mixed approach with small water areas. Due to the increasing number of elements for the larger water areas, the situation changes for water areas with $d_{\mathrm{w}} \geq 10$ m. The same holds for the memory consumption

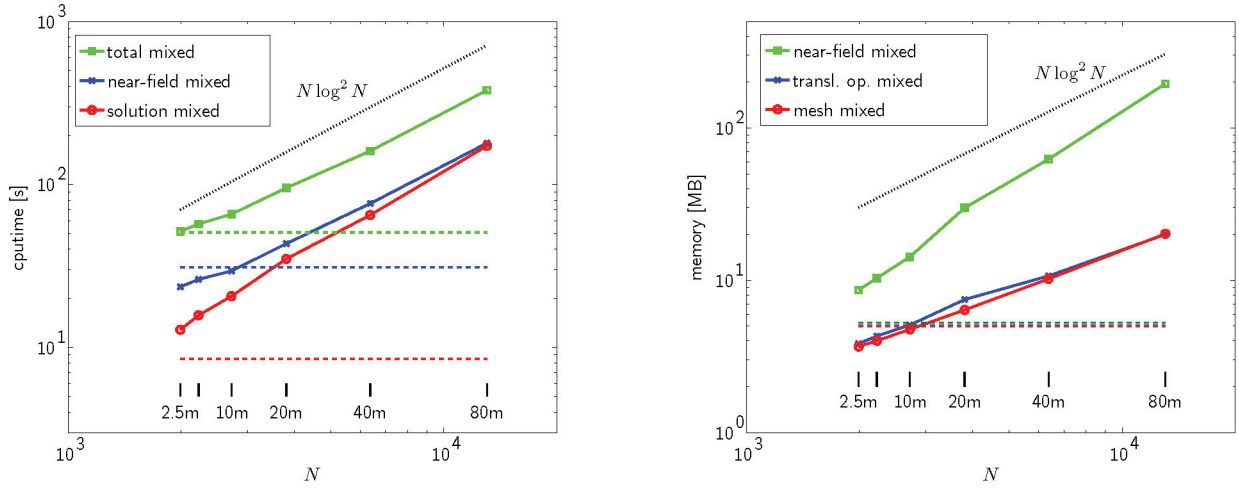

Figure 5: Computation time (left) and memory consumption (right) for the mixed formulation and different water areas with varying number of unknowns N. The corresponding values of the half-space formulation are indicated by dashed horizontal lines of the same color.

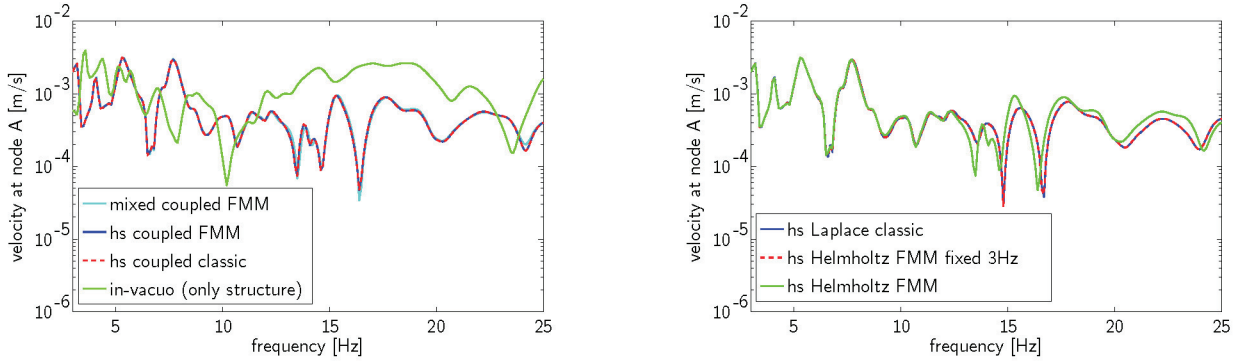

Figure 6: Velocity for the mixed and half-space (hs) formulation for the Helmholtz equation (left). Comparison of the velocity results for the Laplace and Helmholtz equation in case of the coupled half-space formulation (right).

of the translation operators and near-field signatures. One concludes, that the overall memory consumption is smaller for the half-space formulation if not the smallest water area is chosen which yields inaccurate results.

So far, only the fluid part was investigated. In the next subsection, the coupled results are presented.

7.2 COUPLED SIMULATIONS

To compare the coupled simulation results, the velocity at node A (cf. Fig. 3) is investigated. Figure 6 (left) depicts the results for the mixed formulation and the half-space approach. In case of the mixed formulation, the water area is discretized using $d_\mathrm{w} = 10\,\mathrm{m}$. Both implementations use the fast multipole method with the parameters mentioned above. The two graphs show hardly any differences. Only a slight deviation is observed at about 24 Hz. To show the correctness of the results, also the half-space formulation with classical implementation is plotted and shows a good agreement compared to the FMM version. To demonstrate the necessity of a fully coupled scheme, also the pure structural solution is plotted, which neglects the feedback of the acoustic pressure. Obviously, there is a significant difference and one concludes that the forces due to the acoustic pressure have to be taken into account.

So far, only the Helmholtz equation has been considered. It includes the so-called hydromass effect and also the sound radiation into the water. The frequency dependent Helmholtz equation can be replaced by the frequency independent Laplace equation, if only the hydromass effect is of significance and the water is assumed to be incompressible. To examine the influence of the compressibility, the velocity results at node A are shown in Fig. 6 (right). In the low frequency regime, the results of the Laplace equation and the Helmholtz equation are identical. For this reason, it is also possible to apply the Helmholtz equation and only perform one integration at a fixed frequency of 3 Hz. For higher frequencies, the results of this fixed Helmholtz approach are equivalent to the Laplace equation. However, above 12 Hz one observes slight differences

between the Laplace and the Helmholtz equation. For higher frequencies, one expects an increasing influence. However, the structural discretization of the used model is not sufficient for this frequency regime. Hence, such test could not be performed with this model.

8 CONCLUSION

When dealing with ship vibrations, the influence of the surrounding water on the structure has to be considered. In this work, two boundary element methods in combination with a strong coupling scheme are compared. To overcome the restrictions caused by the fully populated matrices of classical boundary element methods, the fast multipole method is applied. A mixed approach, where a part of the water surface is discretized is compared with a half-space approach, where a discretization of only the ship hull is sufficient. The latter one turns out to be superior in accuracy, computation time and memory consumption. Additionally, the influence of the compressibility of the water is investigated by comparing the results for the Laplace equation and the Helmholtz equation. One observes almost identical results in the low frequency regime. For higher frequencies, slight differences are visible.

9 ACKNOWLEDGEMENT

Funding of this project by the German Research Foundation (DFG) under the grant SFB404/T3 is gratefully acknowledged.

References

[1] Amini, S., Harris, P., and Wilton, D. *Coupled Boundary and Finite Element Methods for the Solution of the Dynamic Fluid-Structure Interaction Problem*. Springer Berlin, 1992.

[2] Brunner, D., Junge, M., and Gaul, L. A comparison of FE-BE coupling schemes for large scale problems with fluid-structure interaction. *Int. J. Numer. Meth. Eng. in press, DOI: 10.1002/nme.2412* (2008).

[3] Brunner, D., Of, G., Junge, M., Steinbach, O., and Gaul, L. A fast BE-FE coupling for partly immersed bodies. *Int. J. Numer. Meth. Eng.* (in preparation).

[4] Coifman, R., Rokhlin, V., and Wandzura, S. The fast multipole method for the wave equation: A pedestrian description. *IEEE Antenn. Progag. M. 35* (1993), 7–12.

[5] Fahy, F. *Sound and Structural Vibration: Radiation, Transmission and Response*. Elsevier Press, Amsterdam, Heidelberg, 2007.

[6] Fischer, M. *The Fast Multipole Boundary Element Method and its Application to Structure-Acoustic Field Interaction*. PhD thesis, University of Stuttgart, 2004.

[7] Gaul, L., Kögl, M., and Wagner, M. *Boundary Element Methods for Engineers and Scientists. An Introductory Course with Advanced Topics*. Springer Berlin, 2003.

[8] Gumerov, N., and Duraiswami, R. *Fast Multipole Methods for the Helmholtz Equation in Three Dimensions*. Elsevier, Oxford, 2004.

[9] Gyure, M., and Stalzer, M. A prescription for the multilevel Helmholtz FMM. *IEEE Comput. Sci. Eng. 5* (1998), 39–47.

[10] Hughes, M., and Chen, K. An efficient preconditioned iterative solver for solving a coupled fluid structure interaction problem. *International Journal for Computer Mathematics 81* (2004), 583–594.

[11] Junger, M., and Feit, D. *Sound, Structures, and Their Interaction: Basic Concepts*, 2nd ed. The MIT Press, 1986.

[12] Rjasanow, S., and Steinbach, O. *The Fast Solution of Boundary Integral Equations*. Springer New York, 2007.

[13] Rokhlin, V. Diagonal forms of translation operators for the Helmholtz equation. *Appl. Comput. Harmon. A. 1* (1993), 82–93.

[14] Seybert, A., and Wu, T. Modified Helmholtz integral equation for bodies sitting on an infinite plane. *J. Acoust. Soc. Am. 85* (1989), 19–23.

[15] Stephan, E. Boundary integral equations for mixed boundary value problems in $\mathbb{R}^3$. *Math. Nachr. 184* (1987), 21–53.

[16] Wu, T. *Boundary Element Acoustics. Fundamentals and Computer Codes*. WIT Press Southampton, 2000.

[17] Zienkiewicz, O., and Taylor, R. *The Finite Element Method, Volume 1: The Basis*. Butterworth Heinemann Oxford, 2000.